Genetic Parameter Identification of the Doyle-Fuller-Newman Model from Experimental Cycling of a $LiFePO_4$ Battery

Joel C. Forman, Scott J. Moura, Jeffrey L. Stein, and Hosam K. Fathy*

Abstract*— This paper examines the identification of the parameters of the Doyle-Fuller-Newman electrochemistry-based Lithium-ion battery model from voltage and current cycling data. The battery used in this study has a lithium iron phosphate cathode chemistry intended for high-power applications such as plug-in hybrid electric vehicles. The variables optimized for model identification include parameterizations of the model's anode equilibrium potential, cathode equilibrium potential, and solution conductivity. A genetic algorithm is used to optimize these model parameters against experimental data. The resulting identified model fits two experimental data sets used for system identification, as well as separate validation data sets corresponding to five different vehicle drive cycles. These drive cycles simulate the current a battery would undergo while used in a plug-in hybrid vehicle battery pack. The accuracy of the parameters is investigated using various validation data sets. This is believed to be the first attempt at fitting nearly all of the parameters and functions in the DFN model simultaneously using only voltage and current data. Computational logistics of using a genetic algorithm to identify 88 parameters of an electrochemistry-based model for 7.5 hours of cycling data are discussed. In addition, a detailed analysis of local parameter identifiability is presented.

I. Introduction

THIS paper examines the problem of identifying the parameters of the electrochemical battery model developed by **D**oyle, **F**uller, and **N**ewman (**DFN**) [1-2] using noninvasive voltage-current cycling experiments. The paper uses a genetic algorithm to match the model's voltage predictions to experimental measurements, for a given input current profile. This genetic algorithm optimizes 88 parameters of the DFN model, including parameterizations of the anode and cathode equilibrium potential functions as well as a parameterized solution conductivity function. The end result is an identified model that predicts cell voltage and power within 5% relative error for all of the identification and validation data sets examined in this work. For all of the validation cycles aggregated together the 50th percentile of voltage error is 18.2mV and the 90th percentile of voltage error is still only 54.8mV. This high level of accuracy justifies the use of the DFN model for the lithium-iron-phosphate ($LiFePO_4$) chemistry examined in this work. All of the validation data sets are based on simulated currents that a **P**lug-in **H**ybrid **E**lectric **V**ehicle (**PHEV**) battery pack would experience during driving. Additionally, this paper presents a study of the local identifiability of the DFN model parameters along with the computational logistics involved in using a **G**enetic **A**lgorithm (**GA**) for parameter identification.

The literature already examines battery parameter identification using a number of different models, identification methods, and parameter sets. Santhagopalan *et al.*, for instance, successfully identify a subset of the DFN model parameters using extended Kalman filtering [3]. Speltino *et al.* successfully identify the parameters of a **S**ingle **P**article **M**odel (SPM) of battery dynamics by splitting these parameters into two sets and identifying these sets sequentially [4]. Schmidt *et al.* also successfully identify an SPM battery model, with several extensions that incorporate temperature information and relate solid diffusion to state of charge [5]. The study by Schmidt *et al.* also examines parameter identifiability using Fisher information [5]. Finally, Hu *et al.* successfully identify the parameters of an equivalent circuit battery model using a GA [6].

The above studies have all either identified a small subset of parameters from the DFN model or a simplified version of the model. In contrast, our overarching goal in this paper is to identify the full DFN model from input-output voltage and current data. This is believed to be the first attempt at fitting nearly all of the parameters and functions in the DFN model simultaneously using only voltage and current data. We pursue this goal for an ANR26650M1A battery cell with a $LiFePO_4$ cathode intended for transient power applications such as PHEV propulsion. We perform the fitting using two sets of experimental data: *(i)* a **C**onstant **C**urrent **C**onstant **V**oltage (**CCCV**) charge/discharge sequence and *(ii)* a charge/discharge profile corresponding to a naturalistic PHEV drive cycle. We then validate the resulting identified model using five additional charge/discharge profiles obtained by simulating a PHEV powertrain for both naturalistic and certification drive cycles. Current was treated as the input to both the battery experiments and DFN model in all of these tests, and voltage was treated as the output.

Manuscript received September 22, 2010. This work was supported in part by the National Science Foundation's EFRI-RESIN Grant 0835995.

J. C. Forman is a graduate student at The University of Michigan, Ann Arbor MI 48109 USA (email: jcforman@umich.edu).

S. J. Moura is a graduate student at The University of Michigan, Ann Arbor MI 48109 USA (email: sjmoura@umich.edu).

J. L. Stein is a professor of mechanical engineering at The University of Michigan, Ann Arbor MI 48109 USA (email: stein@umich.edu).

H. K. Fathy is an assistant professor of mechanical engineering at The Pennsylvania State University, University Park, PA 16802 USA (email hkf2@psu.edu). *Address all correspondence to this author.

Successfully matching a given battery cell's voltage response to input currents does not guarantee that all the parameters of the DFN model are identified correctly. This paper uses local identifiability analysis to show that 60 of the DFN model's 88 parameters are *locally identifiable* (with a condition number of 10^{-15}) given the parameter values at the end of the optimization and the specific current histories used for optimization. The fact that these 60 parameters are *identifiable* means that they affect the DFN model's input-output behavior in unique and significant ways that make it possible to identify them from experimental data. The remaining 28 parameters lack this *identifiability* property: a fact that has two key implications. First, the values of these unidentifiable parameters cannot be correctly estimated from the experiments used in this study. Second, errors in the values of these unidentifiable parameters do not affect the validity of the identified DFN model for the input-output conditions examined in this study.

In summary, this paper makes two novel contributions to the literature. It identifies the parameters of the DFN model using noninvasive current-voltage measurements, for the first time. Furthermore, it uses a rigorous local identifiability analysis to assess the accuracy of the resulting parameter values. The remainder of the paper is structured as follows. Section *II* describes the experiments used for identifying the DFN model. Section *III* summarizes the model and describes the approach used for simulating it. Sections *IV* and *V* describe the genetic optimization of the model and parameter set used in this optimization, respectively. Section *VI* presents validation studies for the identified model. Finally, Section *VII* presents the local identifiability analysis and Section *VIII* summarizes the paper's conclusions.

II. Experimental Setup

Fitting and validation data sets have been collected experimentally for ANR26650M1A battery cells with $LiFePO_4$ cathode material. These cells have a 2.3A-h nominal capacity when fresh, a nominal voltage of 3.3V, and a maximum continuous discharge current of 70A (30.4 C-rate). The cells are intended for transient high-power applications including commercial PHEVs, PHEV conversion kits, and portable power tools.

Experimental cycling data have been collected using a custom-built battery tester. This tester is capable of highly transient current/voltage profiles and can switch quickly between charging and discharging. These characteristics make it ideal for testing batteries under conditions similar to those experienced in PHEV battery packs. Additionally, this setup is capable of battery-in-the-loop experimentation, which will be advantageous for future battery control and estimation studies [8].

The above battery tester combines three major hardware components: an electric load (SLH-60-120-1200), a power supply (DSC20-50E), and a **R**eal-**T**ime (**RT**) controller and I/O board (DSC1104). Figure 1 is a photograph of the battery tester, and Fig. 2 is a schematic of the setup where all signal lines are connected to the I/O board. The power supply and electric load handle battery charging and discharging, respectively. The RT I/O board coordinates the electric load, power supply, and switching board. In addition, the RT I/O board records sensor signals including voltage, current, and temperature. These signals are exchanged among the setup's various components in a variety of formats, including the analog, digital, PWM, SMBus, RS-232, and TTL formats. The switch board switches the setup between charging and discharging by swapping the battery's connection between the power supply and load. The Schottky diode protects the power supply from absorbing battery energy. The battery sensor board measures battery voltage through a voltage-isolating differential op-amp, and measures battery current via a bi-directional ±20A Hall effect sensor (ACS714). An infrared thermopile (MLX90614) measures battery temperature. Finally, all the battery interface electronics are implemented on custom-build **P**rinted **C**ircuit **B**oards (**PCBs**) to maximize overall setup reliability, especially for long-term tests.

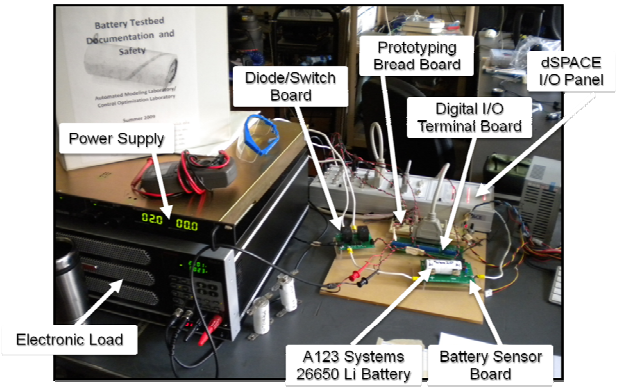

Fig. 1. Photograph of Experimental Battery Tester

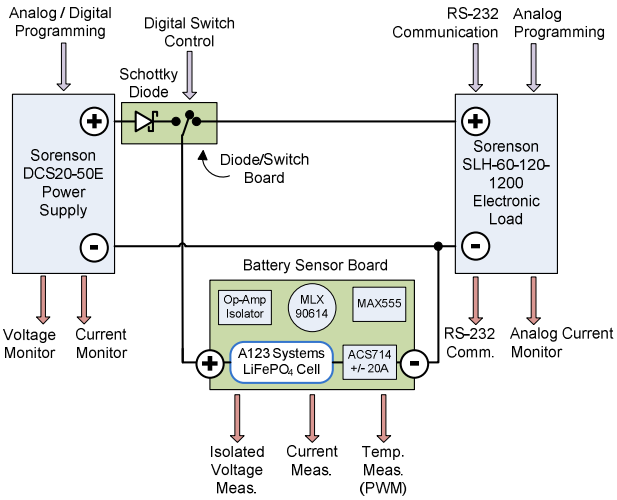

Fig. 2. Schematic of Experimental Battery Tester

Seven battery cycling tests were conducted using the above setup: two for model identification, and five for validation. All of the tests involved initializing battery state of charge to 90% (3.35V relaxed), then subjecting the battery to a given current profile and measuring the resulting battery voltage. In the first identification data set, the current profile

consisted of *"Chirp"* sequence of three CCCV charge/discharge patterns between 2.0V and 3.6V, with charge/discharge rates of 5C, 2.5C, and 1C. In all six remaining tests, the current profile was generated by simulating a PHEV powertrain for some given vehicle drive cycle (i.e., velocity-versus-time profile). Two of these vehicle drive cycles corresponded to the morning and evening commutes of a real human driver in a naturalistic driving study by the **U**niversity of **M**ichigan **T**ransportation **R**esearch **I**nstitute (**UMTRI**) [9]. We will denote the corresponding battery tests by *Naturalistic1* and *Naturalistic2*, respectively. Each of the remaining 4 battery tests corresponded to multiple repetitions of a standard vehicle certification drive cycle. We will denote these battery tests by *UDDSx2, US06x3, SCO3x4,* and *LA92x2*, where the number in *"x#"* refers to the number of drive cycle repetitions. For each of these drive cycle-based battery tests, we simulated a mid-size power-split sedan PHEV with a previously-optimized power management algorithm [10] to translate the vehicle drive cycles to battery current profiles. The PHEV's battery pack size was set to 5kWh for consistency with existing PHEV conversion kits. Due to sensor limitations, drive cycles that produced current magnitudes greater than 20A were scaled down to 20A: *US06x3, SCO03x2*, and *LA92x2*. Finally, we applied the resulting current profiles to the battery cell, thereby obtaining rich data sets for identification and validation.

III. The Doyle-Fuller-Newman Battery Model

The DFN model is an electrochemical battery model that models concentration and potential distributions across the width of the cell as well as concentration profiles in the porous electrodes of the anode and cathode. Spatial distributions across the width of the cell play an important role in high-rate charge and discharge dynamics, typical of PHEV cycles. The model is described thoroughly in [1-2]. The remainder of this section will provide a brief overview of the mathematics involved in this model.

The diffusion of Lithium ions within the electrolyte is governed by Fick's law of linear diffusion combined with an intercalation current density term, *J,* transferring Li-ions between the solution and solid:

$$\varepsilon_2 \frac{\partial c_2}{\partial t} = \nabla \cdot \left(d_2^{eff} \nabla c_2 \right) + \frac{1 - t^+}{F} J \qquad (1)$$

The above intercalation current density, *J*, also acts as an input to the dynamics of Li-ion diffusion within the solid. This diffusion occurs at every point in the anode and cathode and can be modeled using a spherical, radially symmetric diffusion law as follows:

$$\frac{\partial c_{1,j}}{\partial t} = \frac{D_{1,j}}{r^2} \frac{\partial}{\partial r} \left(r^2 \frac{\partial c_{1,j}}{\partial r} \right) \qquad (2)$$

The total intercalation current density, *J*, equals the main intercalation reaction current density, J_1, plus any additional intercalation current density J_{sd} representing side reactions in the battery. We neglect such side reactions in this paper, thereby equating *J* and J_1. The main intercalation reaction current density, J_1, is driven by potential differences between the solid and electrolyte solution, and governed by the Butler-Volmer equation:

$$J_1 = a_j i_{0,j} \left[\exp\left(\frac{\alpha_{a,j} F}{\bar{R}T} \eta_j \right) - \exp\left(-\frac{\alpha_{c,j} F}{\bar{R}T} \eta_j \right) \right] \qquad (3)$$

$$i_{0,j} = k_j \left(c_{1,j}^{\max} - c_{1,j}^{S} \right)^{\alpha_{a,j}} \left(c_{1,j}^{S} \right)^{\alpha_{c,j}} \left(c_2 \right)^{\alpha_{a,j}}, \quad j = n, p \qquad (4)$$

The overpotentials in the above equations equal the differences between the solid and solution potentials minus the reference potentials for the main intercalation reaction, which in turn depend on the local states of charge. In other words, the overpotentials are given by:

$$\eta_p = \phi_1 - \phi_2 - u_{pref} \qquad (5)$$

$$\eta_n = \phi_1 - \phi_2 - u_{nref} - \frac{J}{a_n} R_{SEI} \qquad (6)$$

Since the above potentials/overpotentials can change much faster than the Li-ion concentrations, they are typically assumed to respond instantaneously. The solid potential is governed by Ohm's law with a term governing the charge transfer due to intercalation:

$$\nabla \cdot \left(\sigma_j^{eff} \nabla \phi_{1,j} \right) - J = 0 \qquad (7)$$

Similarly, the solution potential is governed by Ohm's law, intercalation current density, and the charge carried by the ions in solution:

$$\nabla \cdot \left(\kappa^{eff} \nabla \phi_2 \right) + J + \nabla \cdot \left(\kappa_D \nabla \ln \left(c_2 \right) \right) = 0 \qquad (8)$$

The above system of equations governs the dynamics of charging and discharging in the Li-ion cell. From a dynamic systems perspective, it is a system of **D**ifferential **A**lgebraic **E**quations (**DAE**s), where the differential equations govern the diffusion dynamics and the algebraic equations constrain the potentials and intercalation current accordingly.

IV. Parameter Optimization Scheme

Two of the battery tests described in Section *II* were used for the DFN model parameter identification results in this paper: *Chirp* and *Naturalistic1*. The *Chirp* cycle makes SoC-dependent and rate-dependent parameters easier to identify by sweeping through the full range of battery states of charge at different charge/discharge rates. Furthermore, the *Naturalistic1* cycle makes parameters associated with battery transients easier to identify due to its relatively rich frequency content. A previous publication by the authors presented preliminary DFN parameter identification results obtained by performing identification using only part of the

Chirp cycle [11]. This paper is unique compared to that publication in its focus on battery parameter identification and its use of richer data sets to obtain a more accurate parameterization of the DFN model.

The parameter identification objective in this study was to minimize the L^2 error between the experimentally measured voltage traces and the DFN-generated voltage traces. We optimized this objective using a genetic algorithm that varied 88 of the DFN model's parameters. Genetic algorithms are well-suited for such large-scale optimization, especially when gradient information is either impossible or difficult to obtain numerically. We ensured the robustness of the genetic algorithm to model failures by using exception handling to remove population members that induced such failures. An example of such a failure is the computation of complex-valued intercalation currents caused by local overfilling of lithium.

The GA used in this study performed optimal parameter identification as follows. First, it created an initial population of parameter sets randomly. Then it simulated the DFN model for each member of this population (i.e., each parameter set) and assigned a fitness value to this member based on how well it minimized the error between the experimental and simulated voltage traces. Population members were then eliminated randomly through a roulette game weighted by fitness. Elitist selection was used to ensure that the single fittest member was never eliminated. Then new population members were created through the binary mutation and crossover operators. Parents were chosen randomly for crossover, with a selection probability weighted by their fitness. Finally, the new population members' fitness values were computed through DFN model simulation, and the GA iterated till convergence [7].

The above optimization process occurred in the R^{88} Eucledian space, with each parameter quantized at 16 bits. This is a very large optimization space, comprising $7.083*10^{423}$ possible parameter sets. Compounding matters, function evaluations required up to 63 seconds each (function evaluations that failed took less time). The GA was parallelized at the level of simulation function calls, with one server program coordinating multiple quad core computers. This is a typical Master-Slave arrangement. Custom Java computer code handled information exchange over the TCP/IP network within a MATLAB implementation of the GA and DFN model. In practice it took five quad cores (Intel Q8200) about three weeks to perform this optimization. Use of parallel processing was necessary to make this parameter identification problem practical from a numerical standpoint.

V. Parameter Set

This section summarizes the DFN model parameters identified in this paper, and explains some of the constraints placed on these parameters during identification. Altogether, 88 parameters were varied by the genetic algorithm. Five of these parameters pertain to **cell geometry**, namely, the anode thickness L_n, separator thickness L_s, cathode thickness L_p, anode particle radius R_n, and cathode particle radius R_p. These five parameters govern how quickly concentrations can redistribute themselves in the cell. Three parameters govern **ion diffusion rates**, namely, the solid diffusivity d_{1n} in the anode, solid diffusivity d_{1p} in the cathode, and solution diffusivity d_2. One parameter governs the **fraction of the intercalation current carried by Li-ions**, namely, the transference number t^+. Two parameters govern **rate kinetics**, namely, the k-rates k_n in the anode and k_p in the cathode. These multiplicatively affect the current densities generated by the electrochemical reactions. One parameter scales the **solution conductivity and diffusivity** to their effective values, namely, the Brugman number *b*. Three parameters summarize the **cell's porosity**, namely, the solution volume fractions ε_{2n} for the anode, ε_{2s} for the separator and ε_{2p} for the cathode. One parameter captures the effective **impedance of the anode-side solid electrolyte interphase layer**, namely, R_{SEI}. The last scalar parameter was the **initial concentration of the solution**, c_2, which reflects the amount by which the battery is lithiated.

In addition to the above 17 scalar parameters, the GA also optimized the parameters of three curve-fitted functions in the DFN model. Two of these functions were the **equilibrium potential functions**, u_{nref} and u_{pref}, of the anode and cathode, respectively. We represented these functions using 33 control points each, and used monotonic splines to interpolate between these points [12]. The last curve-fitted function was κ^{eff}, which determines the **effective conductivity of the solution as a function of solution concentration**. We represented this function using five control points spaced linearly from 0 mol/m^3 to 4000 mol/m^3, and interpolated between these control points using conventional cubic splines with natural end conditions [13].

Several constraints were placed on the above parameters in the genetic algorithm. First, we constrained the capacity of each electrode to equal exactly 2.7Ah. This constraint provided three key benefits. It eliminated the need for including the maximum concentration c_{1max} in the optimization by making it a function of solid volume fraction, sheet area and electrode width. Furthermore, it created two 0.2 A-h buffers in each electrode, which improved the numerical stability of the DFN model. These buffers add 0.2 A-h of capacity to the maximum and minimum values of the electrodes. This allows the GA to tolerate minor local over and under filling of electrodes as it searches for the correct parameter values. Finally, it eliminated the interplay between changes in electrode charge capacity and changes in equilibrium potential functions versus capacity. The second optimization constraint was to force the three electrode widths (L_n, L_s, L_p) and the area of the sheet rolled up inside the battery to collectively fit within the volume of the battery cell. Constraining the sheet area is particularly important because it acts as a multiplicative scale factor relating applied current to internal current density. The third constraint was to set the volume fractions e_1 and e_2 in the anode and cathode to sum to exactly one. This implies that the vast majority of the battery material

corresponds to either the solid or the solution – which is typical. The final constraint set the solid conductivities σ_{ln} and σ_{lp} to equal 100. This is justified since both conductivities have absolutely zero effect on the voltage trajectory (so long as they are both positive). Not all of these constraints are fully physically justified: a fact that reflects the presence of underlying identifiability issues. This motivates the identifiability analysis in Section *VII*.

VI. Validation Results

The major result of this paper is a set of GA fitted parameter values that match all five validation cycles with high accuracy; see Fig. 3 and Table I. The values of the fitted parameters are given in Tables III and IV. Additional parameters necessary to run the model but not optimized are given in Table II.

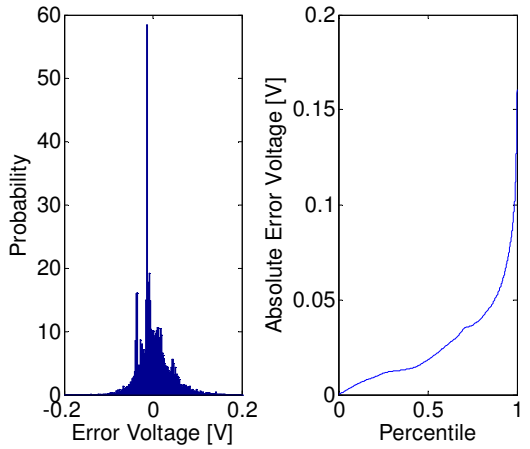

Fig. 3. Probability density plot of voltage error and the percentiles of absolute voltage error for all five of the validation cycles.

TABLE I
PERCENTILE ERRORS OF VOLTAGE (mV)

		Percentile of Error			
		25%	50%	75%	100%
Drive Cycle	*Naturalistic2*	9.6	12.6	14.4	128.6
	LA92x2	13.4	31.1	46.4	160.3
	US06x3	12.7	26.0	46.3	152.6
	SC03x4	11.3	24.0	37.8	158.9
	UDDSx2	12.4	30.1	36.8	152.5
	All Val Cycles	11.1	18.2	36.4	160.3

TABLE II
PARAMETERS NOT INVOLVED IN GA

Name	Value	Unit
c_{1n}	2.479E+04	mol/m^3
c_{1p}	1.649E+03	mol/m^3
c_{1nmax}	2.948E+04	mol/m^3
c_{1pmax}	1.035E+04	mol/m^3
T	2.982E+02	K
α	5.000E-01	-
ε_{1n}	3.810E-01	-
ε_{1p}	4.800E-01	-
σ_n	1.000E+02	1/(mΩ)
σ_p	1.000E+02	1/(mΩ)
Area	3.108E-01	m^2

TABLE III
FIRST HALF OF OPTIMIZED PARAMETERS

			Identifiable @ Condition Number			
Name	Value	Unit	10^-5	10^-10	10^-15	10^-20
L_n	2.885E-05	m	U	I	I	I
L_s	1.697E-05	m	U	U	I	I
L_p	6.521E-05	m	U	I	I	I
R_n	3.596E-06	m	I	I	I	I
R_p	1.637E-07	m	U	U	U	I
t^+	2.495E-01	-	U	U	I	I
b	1.452E+00	-	U	U	I	I
d_2	6.911E-10	m^2/s	U	U	I	I
ε_{2n}	6.190E-01	-	U	U	I	I
ε_{2s}	3.041E-01	-	U	U	I	I
ε_{2p}	5.200E-01	-	U	I	I	I
d_{1n}	8.256E-14	m^2/s	U	U	I	I
d_{1p}	1.736E-14	m^2/s	U	U	U	U
k_n	8.696E-07	(A/m^2) (mol/m^3)$^{1+\alpha}$	U	I	I	I
k_p	1.127E-07	(A/m^2) (mol/m^3)$^{1+\alpha}$	U	U	U	I
R_{SEI}	3.691E-03	Ωm^2	U	I	I	I
c_2	1.042E+03	mol/m^3	U	I	I	I
$u_{nref}1$	3.959E+00	V	U	U	U	U
$u_{nref}2$	3.400E+00	V	U	U	U	U
$u_{nref}3$	1.874E+00	V	U	U	I	I
$u_{nref}4$	9.201E-01	V	U	I	I	I
$u_{nref}5$	9.020E-01	V	U	I	I	I
$u_{nref}6$	6.637E-01	V	U	I	I	I
$u_{nref}7$	2.481E-03	V	U	U	I	I
$u_{nref}8$	1.050E-03	V	U	U	I	I
$u_{nref}9$	1.025E-03	V	U	U	I	I
$u_{nref}10$	8.051E-04	V	U	U	I	I
$u_{nref}11$	5.813E-04	V	U	U	I	I
$u_{nref}12$	2.567E-04	V	U	U	I	I
$u_{nref}13$	2.196E-04	V	U	U	I	I
$u_{nref}14$	1.104E-04	V	U	U	I	I
$u_{nref}15$	3.133E-06	V	U	U	U	I
$u_{nref}16$	1.662E-06	V	U	U	U	I
$u_{nref}17$	9.867E-07	V	U	U	U	I
$u_{nref}18$	3.307E-07	V	U	U	U	U
$u_{nref}19$	1.570E-07	V	U	U	U	U
$u_{nref}20$	9.715E-08	V	U	U	U	U
$u_{nref}21$	5.274E-09	V	U	U	U	U
$u_{nref}22$	2.459E-09	V	U	U	U	U
$u_{nref}23$	7.563E-11	V	U	U	U	U
$u_{nref}24$	2.165E-12	V	U	U	U	U
$u_{nref}25$	1.609E-12	V	U	U	U	U
$u_{nref}26$	1.594E-12	V	U	U	U	U
$u_{nref}27$	1.109E-12	V	U	U	U	U

GA optimized parameter values for the DFN model. Identifiability is given with respect to various condition numbers, I – identifiable, U – unidentifiable.

Relative error in voltage and – consequently – power never exceeds 5% for any of the validation cycles. As shown in Table I, the 50th percentile of voltage error is 18.2mV. Thus, the DFN model can accurately simulate the ANR26650M1A cell for PHEV applications by using this set of parameter values.

The accuracy results of the *Naturalistic2* and *LA92x2* validation cycles are representative of the set of five cycles. *Naturalistic2* is based on recorded data from a real driver's

evening commute. *Naturalistic1* (which was used for fitting) is a morning commute. Figure 5 shows traces of voltage error and Fig. 6 shows traces of power error. Voltage error never exceeds 128.6mV and the 50th percentile of voltage error is 12.6mV. Figure 7 is a probability density plot of the errors along with a percentile plot of errors.

TABLE IV
SECOND HALF OF OPTIMIZED PARAMETERS

			Identifiable @ Condition Number			
Name	Value	Unit	10^-5	10^-10	10^-15	10^-20
$u_{nref}28$	4.499E-13	V	U	U	U	U
$u_{nref}29$	2.250E-14	V	U	U	U	U
$u_{nref}30$	1.335E-14	V	U	U	U	U
$u_{nref}31$	1.019E-14	V	U	U	U	U
$u_{nref}32$	2.548E-16	V	U	U	U	U
$u_{nref}33$	1.654E-16	V	U	U	U	U
$u_{pref}1$	5.502E+00	V	U	U	I	I
$u_{pref}2$	4.346E+00	V	U	I	I	I
$u_{pref}3$	3.676E+00	V	U	I	I	I
$u_{pref}4$	3.537E+00	V	I	I	I	I
$u_{pref}5$	3.494E+00	V	I	I	I	I
$u_{pref}6$	3.409E+00	V	I	I	I	I
$u_{pref}7$	3.388E+00	V	U	I	I	I
$u_{pref}8$	3.380E+00	V	U	I	I	I
$u_{pref}9$	3.379E+00	V	U	I	I	I
$u_{pref}10$	3.335E+00	V	U	I	I	I
$u_{pref}11$	3.331E+00	V	U	I	I	I
$u_{pref}12$	3.330E+00	V	U	I	I	I
$u_{pref}13$	3.328E+00	V	U	I	I	I
$u_{pref}14$	3.316E+00	V	U	I	I	I
$u_{pref}15$	3.307E+00	V	U	I	I	I
$u_{pref}16$	3.297E+00	V	U	I	I	I
$u_{pref}17$	3.295E+00	V	U	I	I	I
$u_{pref}18$	3.293E+00	V	U	I	I	I
$u_{pref}19$	3.281E+00	V	U	I	I	I
$u_{pref}20$	3.270E+00	V	U	I	I	I
$u_{pref}21$	3.261E+00	V	U	I	I	I
$u_{pref}22$	3.257E+00	V	U	I	I	I
$u_{pref}23$	3.255E+00	V	U	I	I	I
$u_{pref}24$	3.242E+00	V	U	I	I	I
$u_{pref}25$	3.233E+00	V	U	I	I	I
$u_{pref}26$	3.213E+00	V	U	I	I	I
$u_{pref}27$	3.197E+00	V	U	I	I	I
$u_{pref}28$	2.927E+00	V	U	I	I	I
$u_{pref}29$	2.847E+00	V	U	I	I	I
$u_{pref}30$	2.828E+00	V	U	I	I	I
$u_{pref}31$	1.026E+00	V	U	U	I	I
$u_{pref}32$	-1.120E+00	V	U	U	U	U
$u_{pref}33$	-1.742E+00	V	U	U	U	U
$\kappa^{eff}1$	1.050E-01	1/(Ωm)	U	U	I	I
$\kappa^{eff}2$	1.760E-01	1/(Ωm)	U	U	I	I
$\kappa^{eff}3$	2.190E-01	1/(Ωm)	U	U	I	I
$\kappa^{eff}4$	8.166E-02	1/(Ωm)	U	U	U	U
$\kappa^{eff}5$	3.014E-02	1/(Ωm)	U	U	U	U

GA optimized parameter values for the DFN model. Identifiability is given with respect to various condition numbers, I – identifiable, U – unidentifiable.

The results for *LA92x2* are very similar to those for *Naturalistic2*. Figures 8 and 9 give the voltage and power trajectories along with their relative and absolute errors. Voltage error never exceeds 160.3mV and the 50th percentile of voltage error is 31.3mV. Figure 10 is a probability density plot of the errors along with a percentile plot of errors.

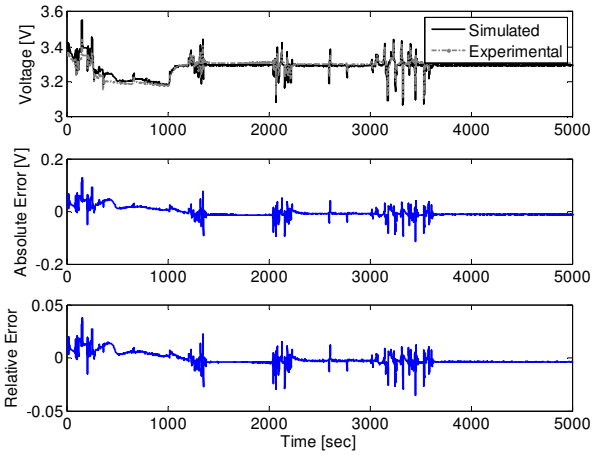

Fig. 5. Voltage Response for *Naturalistic2*.

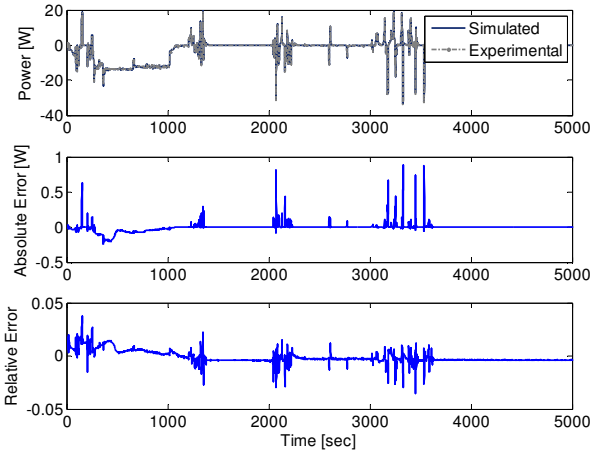

Fig. 6. Power Response for *Naturalistic2*.

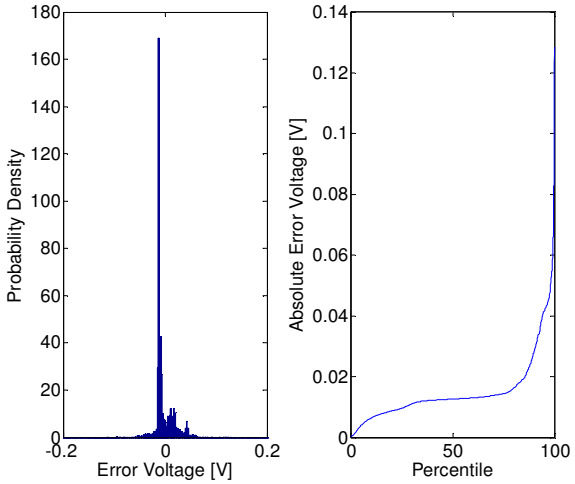

Fig. 7. Probability Density Plot of Voltage Error and the Percentiles of Absolute Voltage Error for *Naturalistic2*

None of the cycles have voltage errors linearly correlated with input current, which implies that the identified model captures at least internal battery resistance very well. Correlation between model error and SoC is low except for *Naturalistic2* which shows some slight correlation (R^2 = 0.577). As a point of comparison the predicted and

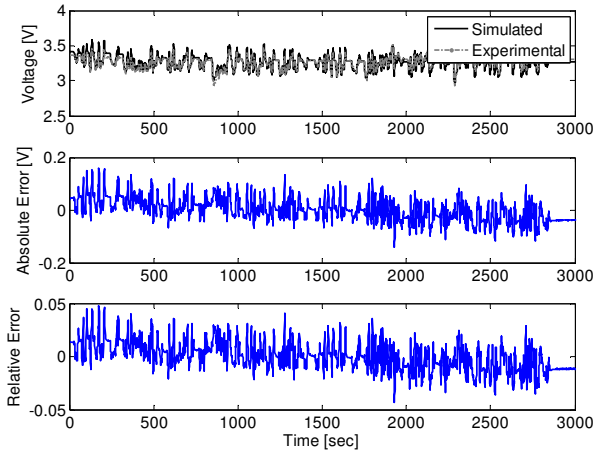

Fig. 8. Voltage Response for *LA92x2*.

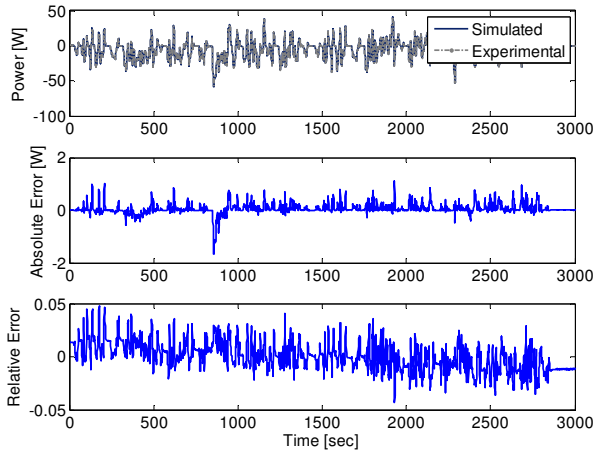

Fig. 9. Power Response for *LA92x2*.

measured voltage for *Naturalistic2* have an R^2 correlation of 0.832. This SoC is the "system" SoC (as opposed to the "chemical" SoC which would be calculated based on the quantity of lithium in the anode) and is calculated for the battery by integrating and scaling current and knowing that each experiment was initialized at 90% SoC. This implies that the identified model captures the dependence of battery dynamics on SoC well. Table V presents the R^2 correlation values for each of the validation cycles.

In summary, this section shows that the DFN model, together with the parameter values identified in this paper, accurately simulates battery cells under the loading characteristics of PHEVs. This accuracy is evident from the small errors in the voltage – and consequently, power – traces of the DFN model compared to experimental data. The parameter values in this paper make it possible to accurately simulate the ANR26650M1A cell for PHEV applications.

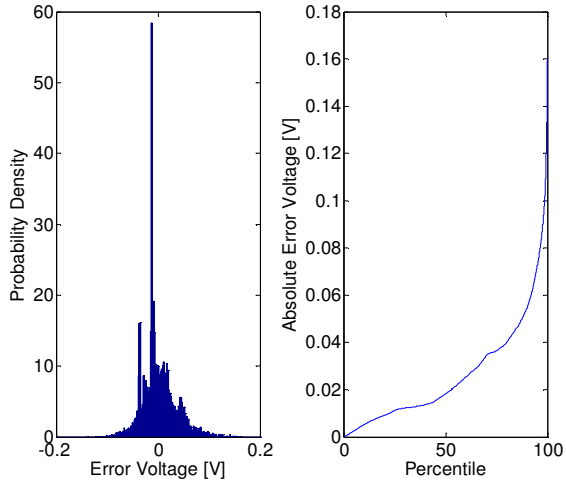

Fig. 10. Probability Density Plot of Voltage Error and the Percentiles of Absolute Voltage Error for *LA92x2*.

TABLE V
R^2 COEFFCIENTS OF CORRELATION WITH ERROR

		I_{app}	SoC
Drive Cycle	*Naturalistic2*	0.048	0.577
	LA92x2	0.085	0.317
	US06x3	0.137	0.333
	SC03x4	0.083	0.298
	UDDSx2	0.067	0.372

VII. Parameter Identifiability

Given the high accuracy of the identified DFN model's voltage and power responses, one might assume that all of the fitted parameter values are the correct physical values. *This assumption is incorrect*. Some of the parameters of the DFN model are locally unidentifiable for the experimental data sets considered in this study. The fact that these parameters are unidentifiable implies that they do not affect the model's input-output characteristics in unique and significant ways. This, in turn, implies that the DFN model identified in this study can accurately predict battery cell behavior for the input-output conditions examined in this study, but must be used with caution for other applications (e.g., non-PHEV applications).

The literature presents at least three definitions of parameter identifiability: global identifiability, structurally local identifiability, and local identifiability [14]. Our goal in this section is to determine which of the DFN model's parameters are locally identifiable for the identification data sets used in this study. To do this, we begin by simulating the DFN model's output voltage response for the optimized parameter values and the identification test data. We denote this voltage response by y_{nom}, and denote the corresponding experimental voltage trace by y_{exper} [14]. The next step is to create an orthogonal basis for the parameter space, inject a slight perturbation along every basis vector, and simulate the resulting perturbation in the DFN model's output from y_{nom}. This furnishes a set of numerical derivatives of the DFN

model's output with respect to its parameters. These derivatives can be stacked into a matrix Y of column vectors – one for each perturbation direction. Once this is achieved, the model's entire parameter set is locally identifiable iff Y^TY has full column rank. If this condition is not satisfied, then one can examine the eigenvalues of Y^TY and choose a cut off value to separate the identifiable and unidentifiable subspaces. In this paper the cutoff value is based on the matrix condition number and four cases are investigated: 10^{-5}, 10^{-10}, 10^{-15}, and 10^{-20} (Fig. 11). One can then project each parameter onto the identifiable subspace to see how much of this vector sits in the space. This can then be used to categorize parameters as identifiable and unidentifiable (with respect to the condition number).

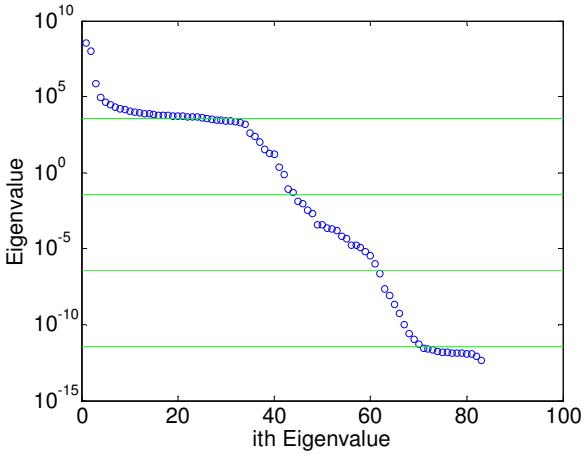

Fig. 11. Eigenvalues of Y^TY and lines for the condition numbers 10^{-5}, 10^{-10}, 10^{-15}, and 10^{-20}.

A semi-log plot of the eigenvalues of Y^TY is given in Fig. 11. If the projection of the parameter unit vector into the identifiable subspace has a length greater than 0.99 then the parameter was considered to be locally identifiable. Tables III and IV present each parameter's identifiability for all four of the condition numbers. For the condition number 10^{-15} all of the scalar parameters are identifiable except for d_{1p}, R_p and k_p - all of which only involve the cathode. For the cathode equilibrium potential, u_{pref}, 31 of the 33 control points were identifiable. For the anode equilibrium potential, u_{nref}, only 12 of 33 control points were identifiable. For κ^{eff}, the solution conductivity as a function of solution concentration, the three control points associated with lower concentrations are identifiable whereas the other two are not. Fortunately the presence of unidentifiable parameters does not affect the quality of the model's response. However it does mean that special care must be taken when using these parameter values for input-output conditions substantially different from those examined herein.

VIII. Conclusions

The DFN model's parameters have been identified for the ANR26670M1A cell using experimental data based on PHEV applications. This fit is accurate with maximum errors for all five validation cycles at less than 5% for power and voltage. For all of the validation cycles aggregated together the 50th percentile of voltage error is 18.2mV and the 90th percentile of voltage error is still only 54.8mV.

The procedure presented makes it possible to find a set of parameter values for the DFN model noninvasively. Unfortunately, this noninvasiveness causes some parameters to lack identifiability. While this does not affect the accuracy of the model response, it does mean that one must be careful when using these parameters in other contexts.

GAs combined with battery experiments have proven to be an effective method for identifying the DFN model's parameter values. This method avoids using invasive electrochemical experiments by using electrical experiments followed by using a computationally intensive GA. As PHEV batteries continue to evolve having a means to identify the DFN parameter values for PHEV batteries will continue to be extremely valuable.

References

[1] M. Doyle, T. Fuller, and J. Newman "Modeling of Galvanostaic Charge and Discharge of the Lithium/Polymer/Insertion Cell," *J. Electrochemical Society*, vol. 140, pp. 1526–1533, June 1993.

[2] T. Fuller, M. Doyle, and J. Newman "Simulation and Optimization of the Dual Lithium Ion Insertion Cell," *J. Electrochemical Society*, vol. 141, pp. 1–10, January 1994.

[3] S. Santhanagopalan, Q. Guo, and R.White "Parameter Estimation and Model Discrimination for a Lithium-Ion Cell," *J. Electrochemical Society*, vol. 154, pp. A198–A206, March 2007.

[4] C. Speltino, D. Domenico, G. Fiengo, and A. Stefanopoulou, "On the experimental identification of an electrochemical model of a lithium-ion battery: Part ii," in *The European Control Conference,* Budapest, 2009.

[5] A. Schmidt, M. Bitzer, A. Imre, and L.Guzzella, "Experiment-driven electrochemical modeling and systematic parameterization for a lithium-ion cell," *J.Power Sources*, vol. 195, pp. 5071–5080, August 2010.

[6] Y. Hu, S. Yurkovich, Y. Guezennec, and B. Yurkovich, "A technique for dynamic battery model identification in automotive applications using linear parameter varying structures," *J. Control Engineering Practice*, vol. 17, pp. 1190-1201, October 2009.

[7] E. Cantú -Paz, *Efficient and Accurate Parallel Genetic Algorithms*. Norwell, MA: Kluwer Academic Publishers, 2000, ch. 3.

[8] H. Fathy, Z. Filipi, J. Hagena, and J. Stein, "Review of hardware-in-the-loop simulation and its prospects in the automotive area," *The International Society for Optical Engineering*, vol. 6228, pp. 1-20, 2006.

[9] D. LeBlanc, J. Sayer, C. Winkler, R. Ervin, S. Bogard, J. Devonshire, M. Mefford, M. Hagan, Z. Bareket, R. Goodsell, and others, "Road Departure Crash Warning System Field Operational Test: Methodology and Results", *University of Michigan Transportation Research Institute*, Tech. Rep. UMTRI-2006-9-1, June 2006.

[10] S. J. Moura, H. K. Fathy, D. S. Callaway, and J. L. Stein, "A Stochastic Optimal Control Approach for Power Management in Plug-in Hybrid Electric Vehicles," *IEEE Transactions on Control Systems Technology*, v PP, n 99, p 1-11, March 2010.

[11] S. Bashash, S. J. Moura, J. C. Forman, and H. K. Fathy, "Plug-in Hybrid Vehicle Charge Pattern Optimization for Energy Cost and Battery Longevity", *Journal of Power Sources*, vol. 196, no. 1, p 541-549, January 2011.

[12] F. Fritsch and R. Carlson, "Monotone Piecewise Cubic Interpolation," *SIAM J. Numerical Analysis,* vol. 17, pp. 238-246, April 1980.

[13] R. Burden and J. Faires, *Numerical Analysis- 7th ed.* Pacific Grove, CA: Wadsworth, 2001, pp. 146–147.

[14] J. Jacquez and T. Perry, "Parameter estimation: local identifiability of parameters," *AJP - Endocrinology and Metabolism*, vol. 258, pp. E727-E736, 1990.